

Iron $K\alpha$ line profiles driven by non-axisymmetric illumination

Qingjuan Yu^{1,2*} and Youjun Lu^{1†}

¹ *Centre for Astrophysics, University of Science and Technology of China, Hefei Anhui 230026, P. R. China*

² *Princeton University Observatory, Princeton, NJ 08544-1001, USA*

Accepted ?. Received ?; in original form May 8, 1998

ABSTRACT

Previous calculations of Fe $K\alpha$ line profiles are based on axisymmetric emissivity laws. In this paper, we show line profiles driven by non-axial symmetric illumination which results from an off-axis X-ray point source. We find that source location and motion have significant effects on the red wing and blue horn of the line profiles. The disk region under the source will receive more flux, which is the most important factor to affect the line profiles. We suggest that at least part of the variation in Fe $K\alpha$ line profiles is caused by the motion of X-ray sources. Future observations of Fe $K\alpha$ line profiles will provide more information about the distribution and motion of the X-ray sources around black holes, and hence the underlying physics.

Key words: galaxies: active – galaxies: nuclei – line: profiles – X-rays: galaxies.

1 INTRODUCTION

The broad Fe $K\alpha$ emission line at 6.4keV in many Seyfert 1 galaxies is a powerful probe of the environment around a black hole. Though its physical mechanism has been interpreted in many ways, recent observations by *ASCA* show that the asymmetric profile of Fe $K\alpha$ emission line is much better explained by gravitational broadening, Doppler effect and accretion-disk origin (Tanaka et al. 1995; Fabian et al. 1995; Nandra et al. 1997; Sulentic et al. 1997 and references therein). Thus, Fe $K\alpha$ line profiles provide a valuable clue to explore the information about the gravitational field, the accretion disk structure, the X-ray continuum source geometry, the inclination between an observer and accretion disk axes and the evidence for the existence of a black hole. Fe $K\alpha$ line profile modeling has attracted much attention and the factors above should be involved in any model based on accretion-disk origin. Theoretical Fe $K\alpha$ line profiles produced in the Schwarzschild metric were first fully relativistically treated by Fabian et al. (1989). Laor (1991) and Kojima (1991) extended those to the Kerr metric. They grasped the two most important physical mechanisms—Doppler effect and gravitational redshift—to produce the Fe $K\alpha$ line profiles, and discussed the important influence of inclination. The detailed structures of the accretion disk/X-ray sources were, however, neglected. Their calculations were formulated on some very simple assumptions, such as the axisymmetric power-law line emissivity law and the Keplerian motion of disk material.

The differences in the line profiles from source to source have implied variations in the geometry and structure of accretion-disk/X-ray source, which cannot be accounted for solely by inclination or the types of central black holes (Nandra et al. 1997). In order to adequately model the Fe $K\alpha$ emission, many detailed calculations about the accretion disk must be performed (Krolik 1996). Considering the geometry (flat, conical or concave), size and ionization state of the accretion disk, some authors have derived more realistic emissivity law by performing Monte Carlo simulations of Compton reflection from a neutral or ionized medium, including fluorescent iron emission (George & Fabian 1991; Matt, Perola & Piro 1991; Matt et al. 1992; Matt, Fabian & Ross 1993b; Życki & Czerny 1994). A more complete calculation was provided by Matt, Fabian & Ross (1996), in which the ionization balance is treated as a function of depth and local angular distribution, and Compton scattering and resonant absorption are taken into account in detail. Some improvement on the kinematics of the accretion disk has also been incorporated into the calculation of Fe $K\alpha$ line profiles. The emitting materials are no longer limited to orbits in the

* Current address: Peyton Hall, Princeton University, Princeton, NJ 08544-1001, USA. E-mail address: yqj@astro.princeton.edu

† E-mail address: lyj@astro.princeton.edu

equatorial plane of a black hole. The effects of the finite thickness, radial accretion flow and turbulence were considered (Pariev & Bromley 1997). Rybicki & Bromley (1997) calculated line formation in the presence of velocity gradients induced by the differential flow in the disk. Recently, Usui, Nishida & Eriguchi (1998) show the Fe $K\alpha$ line profiles from self-gravitating disks or toroids which play an important role for the gravitational field, the dynamics of the disk inner edge and the disk structure.

To date, many authors have incorporated the structure of disks into the calculation of Fe $K\alpha$ lines, but another important factor affecting line profiles—the geometry of X-ray sources, is generally left in an idealized state. The X-ray source is mostly assumed to be a static point located on the disk axis. Matt et al. (1991) extended the source to be a uniform optically thin corona or a homogeneous optically thick sphere to investigate its effects on equivalent width. In that extended-source geometry, the ionization parameter spans a much narrower range of values along disk radii than in the point-source geometry. Matt et al. (1993b) discussed its influences on line profiles, but the disk illumination is still confined to be axisymmetric just as the illumination of an axial point source.

In the past several years, *Ginga* and *GRO OSSE* observation have led to much progress in X-ray source modeling. (Gondek et al. 1996; Zdziarski et al. 1995). Exponentially cut-off power laws of RQ Seyfert 1 X-ray spectra can be modeled by comptonization models either in a non-thermal plasma (Zdziarski, Coppi & Lamb 1990) or in a thermal hot corona covering the disk (Haardt & Maraschi 1991, 1993; Field & Rogers 1993; Zdziarski et al. 1994). Haardt & Maraschi (1991, 1993) presented a uniform, plane-parallel corona and extended it to a patchy structured corona model (Haardt, Maraschi & Ghisellini 1994), since the UV fluxes in many Seyfert 1s are much larger than the X-ray fluxes (Walter & Fink 1993). They proposed that the X-ray emission from radio-quiet active galactic nuclei and galactic black holes is due to comptonization of soft thermal photons emitted by the underlying accretion disk in localized structures. Stern et al. (1995) provided more arguments for the idea that the X-rays come from a number of individual active regions located above the surface of the disk. If so, the flux striking the disk will be determined by the distribution of the blobs and the relativistic motion between the source and the accretion disk. The illumination is not uniform and it depends not only on disk radii but also on polar angles of the disk plane, which will affect the Fe $K\alpha$ line profile because the different energy parts of the Fe $K\alpha$ line profile stem from different angular and radial regions of an accretion disk due to Doppler effect and gravitational broadening (e.g. Matt, Perola & Stella 1993a).

In this paper, we will focus on how the location and motion of one off-axis X-ray source affect the time-averaged Fe $K\alpha$ line profile. We consider an accretion disk around a Schwarzschild black hole. We assume that the disk is illuminated only by one off-axis point source. The flux striking the accretion disk, which is non-axisymmetric, drives the iron line fluorescence. Our results will show the information about the distribution and motion of the X-ray sources can be extracted from the Fe $K\alpha$ line profiles.

2 DISK-LINE IN THE SCHWARZSCHILD METRIC

In the Schwarzschild metric, the line element is written as follows:

$$ds^2 = -(1 - 2/r)dt^2 + \frac{1}{1 - 2/r}dr^2 + r^2d\theta^2 + r^2\sin^2\theta d\varphi^2. \quad (1)$$

where we use the units of $G = c = M = 1$ (M is the black hole mass).

The observer is assumed to be located at $(r_{\text{obs}}, \theta_{\text{obs}}, \varphi_{\text{obs}})$ where $r_{\text{obs}} = 1000$ and $\varphi_{\text{obs}} = 0^\circ$. We set the X-ray point source at $(r_s, \theta_s, \varphi_s)$. We define frames locally moving with the disk materials as R^* (see Appendix). All terms computed in those frames are labeled with a star.

2.1 Photon motions in the Schwarzschild metric

The photons follow null geodesics either between the disk and the X-ray source or between the disk/X-ray source and the observer (Carter 1968; Misner, Thorne & Wheeler 1973). In the Schwarzschild metric, the expressions are simplified as:

$$r^2 \frac{dr}{d\lambda} = \pm EV_r^{1/2} \quad (2)$$

$$r^2 \frac{d\theta}{d\lambda} = \pm EV_\theta^{1/2} \quad (3)$$

$$r^2 \frac{d\varphi}{d\lambda} = \frac{El}{\sin^2\theta} \quad (4)$$

$$r^2 \frac{dt}{d\lambda} = \frac{Er^4}{r^2 - 2r} \quad (5)$$

$$V_r = (r^2)^2 - (r^2 - 2r)(l^2 + q^2) \quad (6)$$

$$V_\theta = q^2 - l^2 \text{ctg}^2 \theta \quad (7)$$

where E , q , l are motion constants and λ is an affine parameter related to the proper time.

Then, the photon motion equations are given by:

$$\int \frac{dr}{V_r^{1/2}} = \pm \int \frac{d\theta}{V_\theta^{1/2}}; \int d\varphi = \pm \int \frac{l d\theta}{\sin^2 \theta V_\theta^{1/2}}. \quad (8)$$

2.2 The observed line flux

Due to relativistic effects, photons emitted with the rest frequency ν_{em}^* will reach the observer with a frequency ν_{obs} , their ratio being given by:

$$g = \frac{\nu_{\text{obs}}}{\nu_{\text{em}}^*} = \frac{\mathbf{p}_{\text{obs}} \cdot \mathbf{u}_{\text{obs}}}{\mathbf{p}_{\text{em}} \cdot \mathbf{u}_{\text{em}}}. \quad (9)$$

We do not consider the effect of higher order images of the disk (Bao, Hadrava & Østgaard 1994a,b). The observed flux distribution $F(E_{\text{obs}})$ at the observed energy is given by (Cunningham 1975):

$$dF(E_{\text{obs}}) = I_{\text{obs}}(E_{\text{obs}})d\Omega = g^3 I_{\text{em}}^*(E_{\text{em}}^*)d\Omega \quad (10)$$

where $d\Omega$ is the solid angle subtended by the disk in the observer's sky and we have made use of the relativistic invariance of I_ν/ν^3 , I_ν being the specific intensity.

Two important ingredients involved in determining the Fe $K\alpha$ emissivity are the structure of the disk and the number of illuminating photons with energy greater than the photoelectric threshold for neutral iron. In this paper, our assumptions about the disk are the same as those in the paper by Reynolds, Young & Begelman et al. (1999). The disk region emitting the iron fluorescence is assumed to be between $r_{\text{in}} = 2$ (the horizon) and $r_{\text{out}} = 200$. Outside the marginally stable orbit r_{ms} ($r_{\text{ms}} \leq r_{\text{em}} \leq r_{\text{out}}$), monochromatic 6.4keV cold Fe $K\alpha$ line is isotropically (in the frame moving with the disk) emitted from the geometrically thin and optically thick disk, where the disk material is essentially in circular, Keplerian motion. Inside the radius of marginal stability, the disk material is assumed to be in free-fall and the line emission is dependent on the ionization parameter ξ . For $\xi \leq 100$ ergs cm s^{-1} , we assume a cold iron fluorescence line at 6.4keV with the strength given by the standard neutral slab calculations. For ξ in the range of 100-500 ergs cm s^{-1} we assume no line emission because of the efficient resonance trapping and Auger destruction of these line photons. For ξ in the range 500-5000 ergs cm s^{-1} we assume a blend of helium-like and hydrogen-like iron line emission with rest frame energies of 6.67 and 6.97 keV, respectively, with an effective fluorescent yield for each line the same as that for the neutral case. For $\xi \geq 5000$ ergs cm s^{-1} , the material is taken to be completely ionized, and no line emission results.

Thus, the specific intensity in the rest frame $I_{\text{em}}^*(E_{\text{em}}^*)$ is given as follows:

$$I_{\text{em}}^*(E_{\text{em}}^*) = \epsilon^*(r_{\text{em}}, \varphi_{\text{em}}) \delta(E_{\text{em}}^* - E_0), \quad (r_{\text{in}} \leq r_{\text{em}} \leq r_{\text{out}}), \quad (11)$$

where $\epsilon^*(r_{\text{em}}, \varphi_{\text{em}})$ is the emissivity law and $E_0 = 6.4, 6.67$ or 6.97 keV depending on r_{em} and ξ . The total observed flux distribution is given by

$$F(E_{\text{obs}}) = \int \epsilon^*(r_{\text{em}}, \varphi_{\text{em}}) g^4 \delta(E_{\text{obs}} - gE_0) d\Omega. \quad (12)$$

The emission is assumed to be isotropic in the source rest frame. In the frame moving with the disk materials, the illumination flux, which is emitted from the X-ray source, is denoted by $F^*(r, \varphi)$. We shall refer to $F^*(r, \varphi)$ as the illumination law. The line enhancement due to the returning radiation (Cunningham 1976; Dabrowski et al. 1997) is neglected. For the matter at a given ionization state, the iron fluorescent emissivity will be proportional to the illumination law, $\epsilon^*(r, \varphi) \propto F^*(r, \varphi)$.

3 CALCULATIONS AND RESULTS

3.1 Non-axisymmetric illumination law

For a X-ray point source on the disk axis or a uniform slab above the disk, the illumination law is generally simplified as axially symmetric, such as r_{em}^q , $H/(r_{\text{em}}^2 + H^2)^{3/2}$ or $H/(r_{\text{em}}^2 + H^2)^{3/2}(1 - 2/r_{\text{em}})^{3+\alpha}$ (Reynolds & Begelman 1997), where H is the X-ray source height above the disk and α is the energy index of the source spectrum $F(\nu) \propto \nu^{-\alpha}$. If the source deviates from the axis, the symmetry will be violated. First, in the Newtonian case, the illumination will become symmetric about the axis joining the source with the point on the disk which is just under the source, not symmetric about the disk axis. Disk regions closer to the source receive more flux, which will be the most important factor resulting in the non-axisymmetric illumination law. Second, at a given radius, the relative motion of the source and each angular region of the disk is no longer

identical, which also cause the asymmetry of the illumination law in the frame moving with the disk materials. In addition, the gravitational lensing effect cannot be neglected. More photons focus towards the black hole. The number of the photons arriving within the range $r_{\text{em}} - r_{\text{em}} + dr_{\text{em}}$ and $\varphi_{\text{em}} - \varphi_{\text{em}} + d\varphi_{\text{em}}$ on the disk will depend not only on r_{em} but also on φ_{em} since the source is off axis. In this paper, using the photon motion equation(8), we take into account both the general and special relativistic effect to work out the time-averaged illumination law (see Appendix A for details). In the calculation, for different source locations and motions, we assume the same X-ray emitting power in the source rest frames, without considering the time differences of the photon motions from the source to the disk.

Fig.1 demonstrates the illuminating flux in the disk material rest frame as a function of r_{em} and $\varphi_{\text{em}} - \varphi_{\text{s}}$ for different locations and motions of X-ray sources. As seen from the figure, the region below the source ($\varphi_{\text{em}} \approx \varphi_{\text{s}}, r_{\text{em}} \approx r_{\text{s}} \sin \theta_{\text{s}}$) receives more flux, which will be the most important factor to affect the Fe K α line profile. At the outer region of the disk, the illumination laws essentially maintain power law of the radii. Since the X-ray source is generally located at the vicinity of the black hole, the illumination at the outer region depends more strongly on the angle $\varphi_{\text{em}} - \varphi_{\text{s}}$ in the inner region than in the outer region. Besides, some features of relativistic effects can be found in the Fig.1. When the source inclination is high (say, $\theta_{\text{s}} = 60^\circ$), the gravitational lensing effect is shown in Fig.1 (a little bump at $\varphi_{\text{em}} - \varphi_{\text{s}} \approx 180^\circ$ in Fig.1j,l,n,p). If the source is static, the photon number striking the disk should be symmetric about $\varphi_{\text{em}} - \varphi_{\text{s}} = 180^\circ$. Including the relativistic effects, the illumination on the receding side to the source ($\varphi_{\text{em}} - \varphi_{\text{s}} \approx 90^\circ$) is generally less than that on the approaching side ($\varphi_{\text{em}} - \varphi_{\text{s}} \approx 270^\circ$) due to Doppler boosting. In addition, it is more realistic that the source has a velocity because the corona in the black hole proximity is generally coupled with the accretion disk via some physical mechanism. For example, Field & Rogers (1993) argued that the corona is magnetically confined by loops of magnetic field which have footprints in the accretion disk. Here, we simply suppose that the source moves with an angular velocity $\mathbf{u}_{\text{s}} = (u_{\text{s}}^t, u_{\text{s}}^r, u_{\text{s}}^\theta, u_{\text{s}}^\varphi) = (u_{\text{s}}^t, 0, 0, u_{\text{s}}^\varphi)$ as the disk materials do (see Appendix). At the very outer radii, that the illumination on the receding side becomes larger than that on the approaching side is just due to the relativistic motion between the source and the disk materials (Fig.1e,g,m,o). That is, the source has a velocity towards the receding side and away from the approaching side.

3.2 Iron K α fluorescent line profiles

Fanton et al. (1997) summarized two integration techniques (direct integration of the geodesic equations and ray tracing) to model emission line profiles. Choosing the ray tracing approach, we use elliptic integrals (Rauch & Blandford 1994) to obtain the Fe K α line profiles with high efficiency. We calculate the trajectories of photons that propagate from the sky plane at the observer to the accretion disk. For each point in the photographic plate of the observer — that is for each impact parameter (α, β)— the constants of motion (l, q) are calculated using the following equations (Cunningham & Bardeen 1973):

$$\alpha = -\frac{l}{\sin \theta}, \beta = (q^2 - l^2 \text{ctg}^2 \theta)^{1/2}. \quad (13)$$

With the equations(8), we can obtain the location $(r_{\text{em}}, \frac{\pi}{2}, \varphi_{\text{em}})$ where the Fe K α line emits with motion constants (l, q). Then by binning the arrived flux at each pixel in the disk image, the emission line profile is obtained using the illumination at $(r_{\text{em}}, \frac{\pi}{2}, \varphi_{\text{em}})$ calculated in Sect.3.1. In this paper, the contribution to the line profile from the region inside the marginally stable orbit is not significant since the source is not set to be very close to the black hole. The contribution from the region $r \leq r_{\text{ms}}$ is significant only when the source is inefficient and close to the black hole.

When the observer inclination is very low (i.e., the disk is face-on), at a given radius, every angular region on the disk almost contributes to the same energy part of the line profile and the frequency shift of the observed photon is approximately only a function of the disk radius r_{em} , not φ_{em} . At its corresponding disk radius, the strength of the line at each frequency is proportional to the integration of illumination over φ_{em} . Thus, the X-ray source geometry affects the line profile simply when the observer inclination is very low. However, when the inclination of the observer is not too low, every part of the line profile corresponds to a certain radial and angular region on the disk (e.g. Matt et al. 1993a). The blue horn comes mainly from the approaching side to the observer and the red part stems from the receding side of the inner disk region. The line profile is affected in a complicated way by the illumination distribution on two parameters r_{em} and φ_{em} . In this paper, we focus more on discussing that case. From the results in Sect.3.1, the illumination is non-axisymmetric when the source deviates from the disk axis and more flux arrives at the region below the source. When the source is above the receding side of the disk ($\varphi_{\text{s}} \approx 90^\circ$), the illumination on the approaching side ($\varphi_{\text{s}} \approx 270^\circ$) will be less, which results in weak blue part of the Fe K α line profile. Correspondingly, the red wing of the line profile is strengthened (Fig.2-3). Likewise, when the source is above the approaching side, the blue horn increases and the red wing is weakened. Those results are also consistent with the one that the two-dimensional transfer function becomes a δ function when θ_{s} is high (Reynolds, Young & Begelman (1999)). As seen from Fig.2-3, when the source inclination is high ($\theta_{\text{s}} = 60^\circ$), the blue horn and the red wing both vary with φ_{s} more violently than they do when θ_{s} is low ($\theta_{\text{s}} = 30^\circ$). The reason is that the illumination differences between the approaching and receding side become larger when θ_{s} is high.

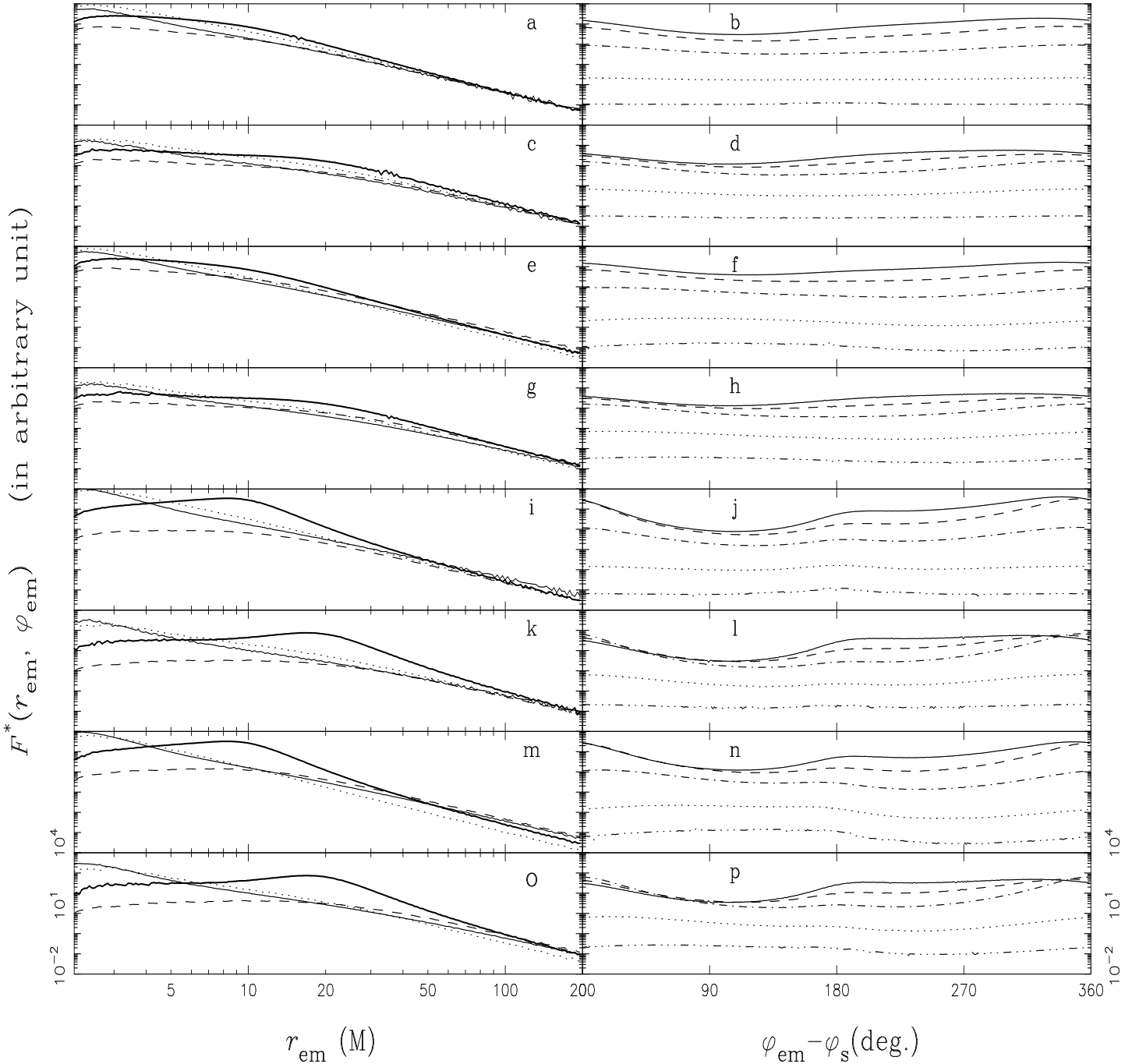


Figure 1. The illumination laws produced by the X-ray point source with different locations and angular velocities (see Appendix): $r_s = 10, \theta_s = 30^\circ, \varpi_s = 0$ (a,b); $r_s = 20, \theta_s = 30^\circ, \varpi_s = 0$ (c,d); $r_s = 10, \theta_s = 30^\circ, \varpi_s = \frac{1}{2}\varpi_{em}(r_s)$ (e,f); $r_s = 20, \theta_s = 30^\circ, \varpi_s = \frac{1}{2}\varpi_{em}(r_s)$ (g,h); $r_s = 10, \theta_s = 60^\circ, \varpi_s = 0$ (i,j); $r_s = 20, \theta_s = 60^\circ, \varpi_s = 0$ (k,l); $r_s = 10, \theta_s = 60^\circ, \varpi_s = \frac{1}{2}\varpi_{em}(r_s)$ (m,n); $r_s = 20, \theta_s = 60^\circ, \varpi_s = \frac{1}{2}\varpi_{em}(r_s)$ (o,p). Left column: $\varphi_{em} - \varphi_s = 0^\circ$ (thick solid line), $\varphi_{em} - \varphi_s = 90^\circ$ (dashed line), $\varphi_{em} - \varphi_s = 180^\circ$ (thin solid line), $\varphi_{em} - \varphi_s = 270^\circ$ (dotted line); right column: $r_{em} = 6.2$ (solid line), $r_{em} = 10.1$ (dashed line), $r_{em} = 20.2$ (dot-dashed line), $r_{em} = 60.0$ (dotted line), $r_{em} = 151.5$ (dot-dot-dot-dashed line).

4 DISCUSSION

The differences in the line profiles from source to source imply variations in the geometry of X-ray sources (Nandra et al. 1997). The variability of some Seyfert 1 galaxies (e.g. MCG-6-30-15, Reynolds & Begelman, 1997) is also explained by the geometry of X-ray sources. In this paper, we explored how the time-averaged line profiles behave for different location and motion of one off-axis source. Generally, the observation angle mainly determines the highest energy that the blue horn can reach. Kojima (1991) examined the difference in the line profiles with different inclination angle, Kerr parameter and disk

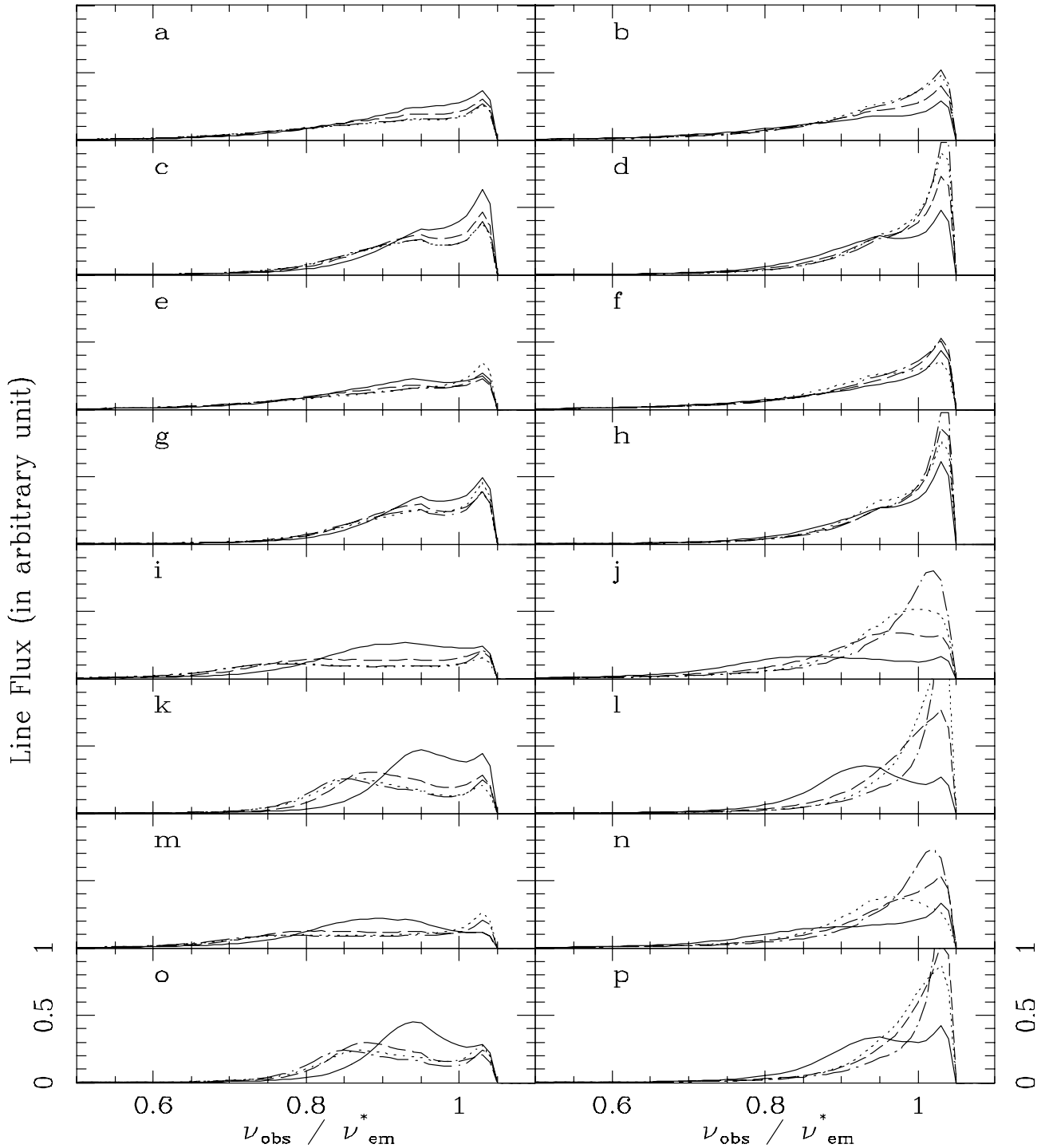


Figure 2. The Fe $K\alpha$ line profiles for different locations and motions of X-ray point sources ($\nu_{em}^* = 6.4\text{keV}$, $r_{obs} = 1000$, $\varphi_{obs} = 0^\circ$). The observer inclination θ_{obs} is 30° . The parameters about the source are the same as those in Fig.1. Left column: $\varphi_s = 0^\circ$ (solid line), $\varphi_s = 45^\circ$ (dashed line), $\varphi_s = 90^\circ$ (dot-dashed line), $\varphi_s = 135^\circ$ (dotted line); right column: $\varphi_s = 180^\circ$ (solid line), $\varphi_s = 225^\circ$ (dashed line), $\varphi_s = 270^\circ$ (dot-dashed line), $\varphi_s = 315^\circ$ (dotted line).

parameters. By comparing the profiles in his paper with the ones in this paper, it is found that at a given source radius and observation angle, the most significant factor affecting the line profiles comes from different X-ray source coordinate φ_s . Moreover, it is more realistic that the source has a velocity u_{φ_s} with the disk materials. The motion of the source will affect the strength of the continuum, too. If the source is above the approaching part of the disk, the blue peak goes up and the observed X-ray continuum is also Doppler boosted; whereas, when the source is above the receding part, the blue horn goes

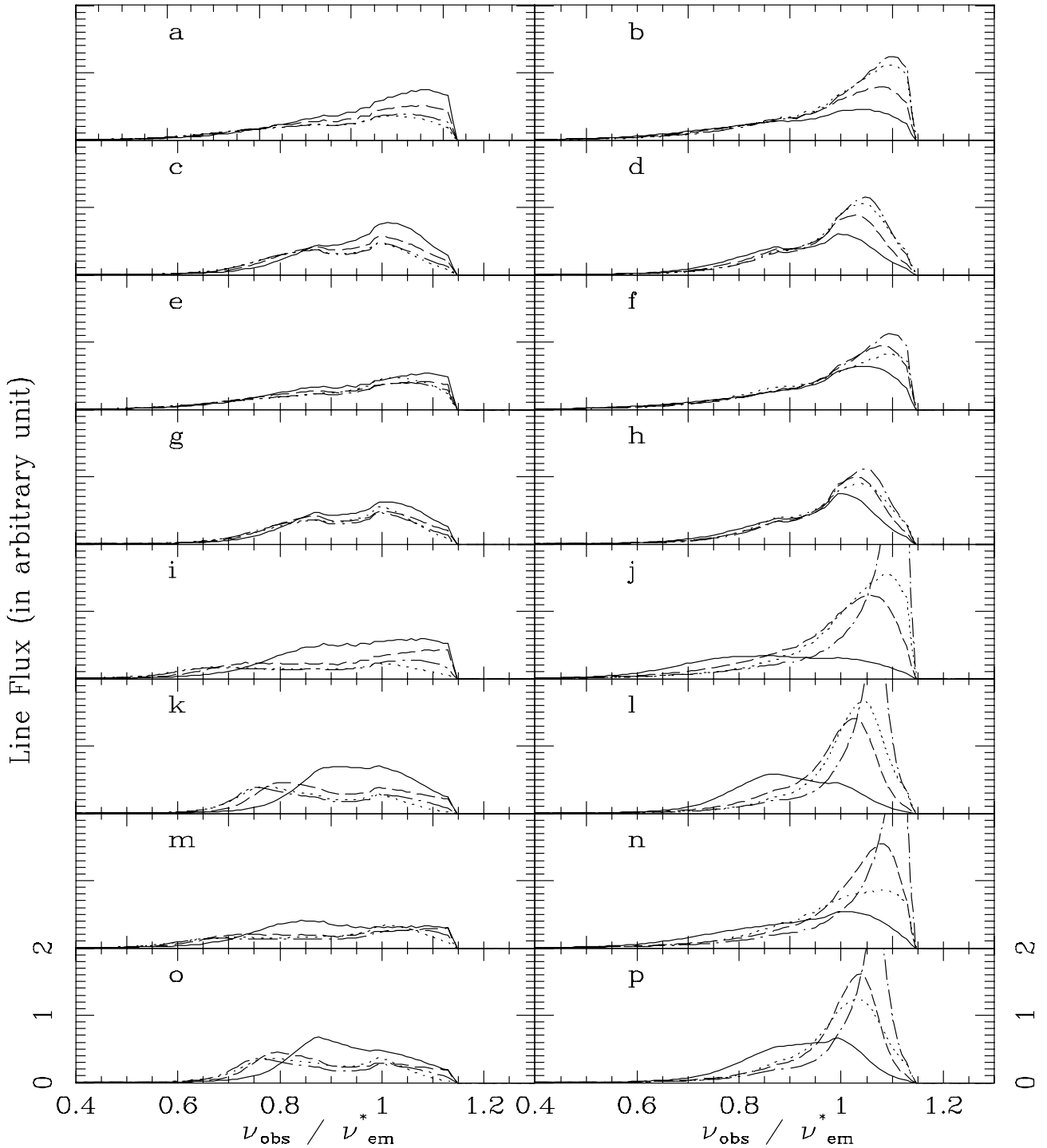


Figure 3. The parameters are the same as those in the Fig.2 except that the observer inclination θ is 60° .

down and the continuum decreases because the source is moving away from us. Those results are also qualitatively true for a Kerr black hole.

There are reasons to believe that in a physically realistic situation, there are a number of active regions or blobs in the patchy corona, rather than one off-axis point source, which collectively drive the iron fluorescence (Haardt, Maraschi, & Ghisellini 1994). The iron line profiles may provide some information about the distribution of those X-ray blobs. The disk regions below those discrete blobs will receive more flux to emit iron fluorescence. It has been pointed out that the Fe $K\alpha$ line profiles of some Seyfert 1 galaxies (say, MCG-6-30-15) are perhaps combined with different components (Sulentic et al. 1998). Here, we suppose that the different components may correspond to the discrete blobs. If there are many blobs in the

corona, the addition of these numerous blobs' illumination may be similar to the results from a uniform thin corona (Matt et al. 1991). While, if there are only several blobs, the addition of those blobs' illumination should still be non-axial symmetric. The flux of the blue horn will be much more correlated with the number and the motion of the blobs above the approaching side of inner disk region; while, the red wing will reflect the state of blobs above the receding side of disk.

Based on the calculation of the off-axis illumination, we suggest that the location and hence the motion of the X-ray source is an alternative explanation for the variation and reddening of the Fe K α line profile. Indeed, it is more realistic that the X-ray source moves near the central black hole. Such an explanation of Fe K α variability can naturally explain the variability time-scale. We can conclude that at least part of the variation of Fe K α line is caused by the motion of the X-ray source. In order to understand the motion of the X-ray source, we should consider both the time difference of the photon motions from the flare to the disk and from the disk to the observer instead of the time-averaged line profile presented here. If the source is static or its life-time is very short (say, $< 10^2$ s, for an AGN black hole with $10^7 M_{\odot}$ whose light crossing time of the gravitational radius is 50s), the time-averaged line profile calculated in this paper should reflect the observed time-averaged line profile, which is the time accumulation of the time-dependent profiles. While, if the source is in motion and its life-time (e.g. $> 10^2$ s) is long enough that its location (say, φ_s) significantly changes, the observed time-averaged iron profile should be the integration of the profiles calculated in this paper along the location of the sources in the motion. Detailed calculation should be done for the effects of an off-axis source on the Fe K α line profile and its variation.

Of the future X-ray missions, *Astro-E* has the best energy resolution at the iron K line. *XMM* has the largest effective area and it is more appropriate for detecting the line variability, which can provide the best quality spectra to examine the disk structure, geometry, ionization state, and so on (Kunieda, 1996). Recently, Reynolds, Young & Begelman et al. (1999) calculated the iron line response to the activation/flaring of a new emitting region, which may be used to probe the mass and spin of AGN black holes as well as the X-ray source geometry. Most of their calculations are performed for the case of one on-axis source. The calculation for off-axis and moving off-axis flares should be developed further. The combination of the theoretical calculation and observational data will reveal important clues of the motion of X-ray sources, the X-ray emission mechanism and also the underlying physical process.

5 CONCLUSION

In this paper, we explored the effects on time-averaged iron K α line profiles driven by an off-axis X-ray source. We found different source location and motion have a significant effect on illumination. The disk region under the source will receive more flux, which is the most important factor to affect the line profiles. We suggest that at least part among the variation of Fe K α line profiles is caused by the motion of X-ray source. The time-averaged line profiles can provide information about the distribution and motion of X-ray sources. To reveal more information about the X-ray source nature, time-dependent line profiles should be explored in future work.

ACKNOWLEDGMENTS

We thank the anonymous referee for a critical reading of this paper and many useful suggestions. Y. Lu thanks the support of Chinese National Science Foundation and Pan-Deng Project.

REFERENCES

- Bao G., Hadrava P., Østgaard E., 1994a, ApJ, 425, 63
 Bao G., Hadrava P., Østgaard E., 1994b, ApJ, 435, 55
 Carter B., 1968, Phys. Rev., 174, 1559
 Chandrasekhar S., 1983, The Mathematical Theory of Black Holes. Oxford University Press, Oxford, p.68-p.69
 Cunningham C. T., Bardeen J. M., 1973, ApJ, 183, 237
 Cunningham C. T., 1975, ApJ, 202, 788
 Cunningham C. T., 1976, ApJ, 208, 534
 Dabrowski, Y., Fabian A. C., Iwasawa K., Lasenby A. N., Reynolds C. S., 1997, MNRAS, 288, L11
 Fabian A. C., Rees M. J., Stella L., White N. E., 1989, MNRAS, 238, 729
 Fabian A. C., Nandra K., Reynolds C. S., Brandt W.N., Otani C., Tanaka Y., Inoue H., Iwasawa K., 1995, MNRAS, 277, L11
 Fanton C., Calvani M., de Felice F., Čadež A., 1997, PASJ, 49, 159
 George I. M., Fabian A. C., 1991, MNRAS, 249, 352
 Gondek D., Zdziarski A. A., Johnson W. N., George I. M., McNaron-Brown K., Magdziarz P., Smith D., Gruber D. E., 1996, MNRAS, 282, 646
 Haardt F., Maraschi L., 1991, ApJ, 380, L51
 Haardt F., Maraschi L., 1993, ApJ, 413, 507
 Haardt F., Maraschi L., Ghisellini G., 1994, ApJ, 432, L95

- Iwasawa K. et al., 1996, MNRAS, 282, 1038
 Kojima Y., 1991, MNRAS, 250, 629
 Krolik J. H., 1996, in Peterson B.M., Cheng F.-Z., Wilson A. S., eds, A.S.P. Conf. Ser. Vol. 113, Emission Lines in Active Galaxies: New Methods and Techniques. Bookcrafters Inc., p.459-p.473
 Kunieda H., 1996, in Peterson B.M., Cheng F.-Z., Wilson A. S., eds, A.S.P. Conf. Ser. Vol. 113, Emission Lines in Active Galaxies: New Methods and Techniques. Bookcrafters Inc., p.1-p.19
 Laor A., 1991, ApJ, 376, 90
 Matt G., Perola G. C., Piro L., 1991, A&A, 247,25
 Matt G., Perola G. C., Piro L., Stella L., 1992, A&A, 257,63 (*Erratum*: 1992, A&A, 263, 453)
 Matt G., Perola G. C., Stella L., 1993a, A&A, 267,643
 Matt G., Fabian A. C., Ross R. R., 1993b, MNRAS, 262, 179
 Matt G., Fabian A. C., Ross R. R., 1996, MNRAS, 278, 1111
 Misner C. W., Thorne K. S., Wheeler J. A., 1973, Gravitation. Freeman, San Francisco
 Nandra K., George I. M., Mushotzky R. F., Turner T. J., Yaqoob T., 1997, ApJ, 477, 602
 Pariev V. I., Bromley B. C., 1998, ApJ, 508, 590
 Petrucci P. O., Henri G. 1997, A&A, 326, 99
 Rauch K. P., Blandford R. D., 1994, ApJ, 421, 46
 Reynolds C. S., Begelman M. C., 1997, ApJ, 488, 109
 Reynolds C. S., Young A. J., Begelman M. C., Fabian, A. C., 1999, ApJ, 514, 164
 Rybicki G. B., Bromley B. C., 1997, astro-ph/9711104
 Stern B. E., Poutanen J., Svensson R., Sikora M., Begelman M. C., 1995, ApJ, 449, L13
 Sulentic J. W., Marziani P., Zwitter T., Calvani M., Dultzin-Hacyan D., 1997, astro-ph/9712336
 Sulentic J. W., Marziani P., Calvani M., 1998, ApJ, 497, L65
 Tanaka Y. et al., 1995, Nature, 375, 659
 Usui F., Nishida S., Eriguchi Y., 1998, MNRAS, 301, 721
 Walter R., Fink H. H., 1993, A&A, 274, 105
 Zdziarski A. A., Coppi P. S., Lamb D. Q., 1990, ApJ, 357, 149
 Zdziarski A. A., Fabian A. C., Nandra K., Celotti A., Rees M. J., Done C., Coppi P. S., Madejski G. M., 1994, MNRAS, 269, L55
 Zdziarski A. A., Johnson W. N., Done C., Smith D., McNaron-Brown K., 1995, ApJ, 438, L63
 Zycki P. T., Czerny B., 1994, MNRAS, 266, 653

APPENDIX A: CALCULATION OF ILLUMINATION LAWS

The line element in a static axisymmetric space-time can be expressed in this form (Chandrasekhar 1983):

$$ds^2 = -e^{2\nu}(dt)^2 + e^{2\psi}(d\varphi - \omega dt)^2 + e^{2\mu_2}(dx^2)^2 + e^{2\mu_3}(dx^3)^2. \quad (\text{A1})$$

A point in that space-time is assigned the four-velocity:

$$u^0 = \frac{dt}{ds} = \frac{e^{-\nu}}{\sqrt{1-V^2}}, u^1 = \frac{d\varphi}{ds} = \varpi u^0, u^\alpha = \frac{dx^\alpha}{ds} = u^0 v^\alpha (\alpha = 2, 3), \quad (\text{A2})$$

where

$$\varpi = \frac{d\varphi}{dt}, v^\alpha = \frac{dx^\alpha}{dt} (\alpha = 2, 3), \quad (\text{A3})$$

and

$$V^2 = e^{2\psi-2\nu}(\varpi - \omega)^2 + e^{2\mu_2-2\nu}(v^2)^2 + e^{2\mu_3-2\nu}(v^3)^2. \quad (\text{A4})$$

The line element will degenerate into the Schwarzschild metric if

$$e^{2\nu} = 1 - 2/r, e^{2\psi} = r^2 \sin^2 \theta, e^{2\mu_2} = \frac{1}{1 - 2/r}, e^{2\mu_3} = r^2, dx^2 = dr, dx^3 = d\theta, \omega = 0. \quad (\text{A5})$$

For a Schwarzschild black hole, we define R^* as the local frame moving with the disk materials, R as curvature coordinates frame not moving with the disk materials and R' as the local rest frame of the X-ray source. All terms computed in R^* and R' are labeled with a star or prime respectively. In the frame rotating with the disk, including the 'k-correction', the illuminating flux on the disk is given by (Petrucci & Henri 1997):

$$F_{\text{em}}^*(r_{\text{em}}, \varphi_{\text{em}}) = \frac{dP_{\text{em}}^*}{dS_{\text{em}}^*} = \left(\frac{\nu_{\text{em}}^*}{\nu_s'}\right)^{2+\alpha} \left(\frac{dP_s'}{d\Omega_s'}\right) \frac{1}{dS_{\text{em}}^*} \quad (\text{A6})$$

where

ν_s' is the photon frequency in the source rest frame;

ν_{em}^* is the photon frequency in the disk material rest frame;

α is the spectral index of the X-ray continuum $P_s'(\nu_s') \propto \nu_s'^{-\alpha}$ and here we assume $\alpha = 1.0$;

dS_{em}^* is the unit area of the disk in R^* ;

$d\Omega'_s$ is the unit solid angle in R' ;

$\frac{dP'_s}{d\Omega'_s}$ is the emitting power per unit solid angle in R' .

Using the covariance of the space-time quadri-volume between the two inertial frames R and R^* , we have

$$dS_{em}^* dt_{em}^* dh_{em}^* = dS_{em} dt_{em} dh_{em}, \quad (A7)$$

where dh_{em}^* and dh_{em} are the elementary space intervals in the direction of the disk axis. Since there is no motion along this axis, $dh_{em}^* = dh_{em}$; thus

$$F_{em}^*(r_{em}, \varphi_{em}) = \left(\frac{dP'_s}{d\Omega'_s} \right) \frac{d\Omega'_s}{dS_{em}} \frac{dt_{em}^*}{dt_{em}} \left(\frac{\nu_{em}^*}{\nu'_s} \right)^{2+\alpha} \quad (A8)$$

where

$$dS_{em} = \frac{r_{em}}{\sqrt{1-2/r_{em}}} dr_{em} d\varphi_{em}; \quad (A9)$$

$$\frac{dt_{em}^*}{dt_{em}} = \sqrt{1-V_{em}^2}; \quad (A10)$$

$$\frac{\nu_{em}^*}{\nu'_s} = \frac{\mathbf{p}_{em} \cdot \mathbf{u}_{em}}{\mathbf{p}_s \cdot \mathbf{u}_s}; \quad (A11)$$

$$\mathbf{p}_{em} = (p_{t_{em}}, p_{r_{em}}, p_{\theta_{em}}, p_{\varphi_{em}}) \quad (A12)$$

$$= (-E, \pm E \frac{\sqrt{r_{em}^4 - (r_{em}^2 - 2r_{em})(l^2 + q^2)}}{r_{em}^2 - 2r_{em}}, \pm E \sqrt{q^2 - l^2 \text{ctg}^2 \theta_{em}}, El); \quad (A13)$$

$$\mathbf{u}_{em} = (u_{em}^t, u_{em}^r, u_{em}^\theta, u_{em}^\varphi) = (u_{em}^t, 0, 0, \varpi_{em} u_{em}^t); \quad (A14)$$

$$\varpi_{em}(r_{em}) = \frac{1}{r_{em}^{3/2}}; \quad (A15)$$

$\frac{dP'_s}{d\Omega'_s} = \text{constant}$ because that the emission is assumed to be isotropic in the source rest frame.

In the X-ray source rest frame R' , the local emission angles, expressed in spherical polar coordinates, come from projecting \mathbf{p}_s onto the spatial basis vectors:

$$\cos\theta'_s = -\frac{\mathbf{p}_s \cdot \mathbf{e}_{\hat{\theta}_s}}{\mathbf{p}_s \cdot \mathbf{u}_s}, \sin\theta'_s \cos\varphi'_s = -\frac{\mathbf{p}_s \cdot \mathbf{e}_{\hat{r}_s}}{\mathbf{p}_s \cdot \mathbf{u}_s}, \sin\theta'_s \sin\varphi'_s = -\frac{\mathbf{p}_s \cdot \mathbf{e}_{\hat{\varphi}_s}}{\mathbf{p}_s \cdot \mathbf{u}_s}; \quad (A16)$$

$$\mathbf{e}_{\hat{\theta}_s} = \frac{1}{r_s} \partial_{\theta_s}, \mathbf{e}_{\hat{r}_s} = \sqrt{1 - \frac{2}{r_s}} \partial_{r_s}, \mathbf{e}_{\hat{\varphi}_s} = \frac{1}{r_s \sin\theta_s} \partial_{\varphi_s}; \quad (A17)$$

$$\mathbf{u}_s = (u_s^t, u_s^r, u_s^\theta, u_s^\varphi); \quad (A18)$$

$$\mathbf{p}_s = (p_{t_s}, p_{r_s}, p_{\theta_s}, p_{\varphi_s}) \quad (A19)$$

$$= (-E, \pm E \frac{\sqrt{r_s^4 - (r_s^2 - 2r_s)(l^2 + q^2)}}{r_s^2 - 2r_s}, \pm E \sqrt{q^2 - l^2 \text{ctg}^2 \theta_s}, El). \quad (A20)$$

We assume two cases about the motion of the X-ray source: one is that the source is static $\mathbf{u}_s = (u_s^t, 0, 0, 0)$; the other is that the source has an angular velocity $\mathbf{u}_s = (u_s^t, 0, 0, \varpi_s u_s^t)$ as the disk materials since the corona is generally coupled with the accretion disk, where we assume $\varpi_s = \frac{1}{2} \varpi_{em}(r_s) = \frac{1}{2} \frac{1}{r_s^{3/2}}$. The emission is supposed to be isotropic in the source rest frame and photons are uniformly produced within the ranges $\theta'_s \in [-\pi/2, \pi/2]$ and $\varphi'_s \in [0, 2\pi)$. For any given (θ'_s, φ'_s) , the motion constants of photons (l, q) can be derived by the above equations (A16). Using the photon motion equations (8), we will work out whether the photons will arrive at the disk surface and the corresponding coordinates $(r_{em}, \frac{\pi}{2}, \varphi_{em})$ can be calculated. Then, by (A8), the distribution of the illumination flux (Fig.1) can be estimated.